Journal of Sound and Vibration 574 (2024) 118238

Contents lists available at ScienceDirect

Journal of Sound and Vibration

journal homepage: www.elsevier.com/locate/jsvi

Numerical and experimental investigations on quasistatic pulse generation of ultrasonic guided waves in fiber reinforced composite pipes

Chang Jiang [a,b], Weibin Li [b,*], Ching-Tai Ng [a,*], Mingxi Deng [c,*]

[a] School of Architecture & Civil Engineering, University of Adelaide, Adelaide, South Australia, 5005, Australia
[b] School of Aerospace Engineering, Xiamen University, Xiamen, Fujian, 361000, PR China
[c] College of Aerospace Engineering, Chongqing University, Chongqing, 400010, PR China

ARTICLE INFO

Keywords:
Quasistatic pulse
Ultrasound
Guided wave
Material nonlinearity
Composite pipe

ABSTRACT

The quasistatic pulse (QSP) generation of ultrasonic guided waves in composite pipes can exhibit many features that are useful for early-stage material characterization and structural health monitoring. The intrinsic relationship between the QSP generation and the weak elastic nonlinearity of solids is complex. It has yet promised for developing the nonlinear ultrasonic guided wave technique that combines its advantages of high sensitivity to microdamage and low ultrasonic attenuation in composite materials. This study presents a systematic investigation of the QSP generation in fiber reinforced composite pipes. Using a three-dimensional finite element simulation with a nonlinear material model, the temporal waveform, mode conversion effect, cumulative effect, generation efficiency, and duration effect of QSP generation are revealed. The nonlinear QSP signals in laminated composite pipes are confirmed as the fastest wave mode that only has axial displacement. The shape of QSP depends on the group velocity difference between the QSP and the primary wave. The magnitude of QSP is related to the excitation level, frequency, and tone-burst duration of the primary wave. Experiments are conducted using carbon fiber reinforced composite pipes and the signals are measured using a laser vibrometer scanning system for verifying the QSP generation. The experimental results are consistent with the numerical findings. A relative nonlinear acoustic parameter based on the QSP generation is proposed and used to evaluate the early-stage thermal fatigue damage in the pipes. The measured nonlinear acoustic parameter demonstrates high sensitivity to the damage, indicating considerable potential for industrial applications.

1. Introduction

Due to corrosion resistance, lightweight nature, high strength-to-weight ratio, durability, and design flexibility, fiber reinforced polymer (FRP) composites have gained significant interest in various industrial applications [1]. Detecting damage in composites is crucial for ensuring structural integrity in aerospace, automotive, construction, and other fields [2]. Ultrasonic techniques, specifically guided wave (GW) methods [3–5] combined with nonlinear acoustic approaches [6,7], offer advantages such as high sensitivity, deep penetration, portability, and real-time imaging. These methods enhance ultrasound's sensitivity to smaller defects compared to the

* Corresponding authors.
E-mail addresses: liweibin@xmu.edu.cn (W. Li), alex.ng@adelaide.edu.au (C.-T. Ng), mxdeng@cqu.edu.cn (M. Deng).

https://doi.org/10.1016/j.jsv.2024.118238
Received 12 August 2023; Received in revised form 19 December 2023; Accepted 2 January 2024
Available online 7 January 2024

wavelength, while reducing inspection costs for large structures. In industries like pipelines and storage containers, nonlinear ultrasound-based structural health monitoring (SHM) techniques play a more vital role in providing early-stage damage information than conventional nondestructive techniques.

Recent advances in the research and application of nonlinear GW (NGW) mostly involve the measurement of higher harmonic generation [7–9]. However, for detecting material nonlinearity-related damages, higher harmonic generation normally requires satisfaction of synchronism and non-zero power flux conditions [10,11]. The cumulative effect, by which the magnitude of the higher harmonic grows with the propagation distance, benefits the measurement of nonlinear signals. Li et al. [12] used the phase velocity and group velocity matched mode pair for evaluating thermal fatigue damage in metallic pipes. Another study [13] on the nonlinear response of early damage in the inner layer of a composite metallic tube by circumferential GW also involved strict mode selection for achieving cumulative second harmonic generation. However, the appropriate selection of suitable mode pairs usually requires advanced knowledge of dispersion features and vibrational characteristics of GWs. Owing to the complex mechanical properties and damage mechanisms of FRP composites, the process of wave mode selection requires significant effort. A similar situation is encountered when applying GW mixing technique [11,14,15]. Considering the wavelength and mode shape of the GW to be excited, the number of available mode pairs for assessing material nonlinearity-related microdamage is often limited. Apart from the complex dispersion features of GW and damage mechanism in anisotropic composite pipe-like structures, ultrasound attenuation is also one of the key factors in developing a suitable NGW technique. Due to the known exponential attenuation characteristic of ultrasound with respect to frequency (especially strong attenuation effect in composites), the advantage of long propagation distance of GWs is still limited when using higher harmonic generation.

An important aspect of nonlinear ultrasound that has not been studied widely is the generation of the quasistatic pulse (QSP) response of tone-burst GWs. The study on the quasistatic response of GWs origins from the research on acoustic static strain (i.e., DC response) by plane longitudinal waves [16–19]. In the context of classical nonlinear stress-strain relation, the temporal shape of QSP by finite-size longitudinal wave has been confirmed as the envelop-like shape of the fundamental wave, which can also be influenced by boundary conditions. Due to zero frequency of the carrier wave, the QSP generated from ultrasound propagation is traditionally neglected by signal filtering. There has been literature [20,21] reporting the QSP generation of GWs in both isotropic metallic and anisotropic composite materials by numerical studies. The mode of QSP generated by different primary GWs in thin plates has been verified as S0 mode at near-zero frequency with only in-plane displacement. However, as one of the nonlinear responses, the QSP signal usually propagates along the plate with large energy divergence (i.e., the induced QSP has poor directivity due to low frequency). This indicates that ultrasound excitations with large amplitude and higher frequency are desired for effective signal-to-noise ratio (SNR) of practical QSP applications in plate structures. For hollow cylinders, there exists a scarce amount of documentation regarding the QSP generation in pipe structures. In view of the closed cross-sections of tubular waveguides, it is expected that the QSP in pipes has much less energy dissipation than that in plates. An additional advantage of QSP generation is the zero frequency of its carrier wave that can contribute to neglectable acoustic attenuation and a much longer propagation distance than higher harmonics. Furthermore, the QSP as nonlinear signal is typically independent of instrumental nonlinearity and can be detected by either low-frequency transducers or laser vibrometers. Previous studies [22,23] on early damage detection in polymer materials with great ultrasonic attenuation using QSP generation of bulk waves and Lamb waves has shown the high sensitivity of QSP to microscale thermal damage and low velocity impact damage. Thus, the potential of applying QSP generation for the assessment of material nonlinearity and local damages in composite pipes is promising.

The objective of this study is to investigate the generation of QSP in anisotropic FRP composite pipes and further verify the applicability of using QSP of GW for assessing material nonlinearity-related damage in FRP composite pipes. A systematic study on the QSP generation mechanism and propagation characteristics in composite pipes is conducted. To gain insights into the QSP generation in complex FRP pipes, numerical analyses of dispersion characteristics and wave structures of GWs in FRP composite pipes are performed first using the semi-analytical finite element (SAFE) method [24,25] with efficient and accurate frequency-domain numerical results. Moreover, a three-dimensional (3D) finite element (FE) model is developed considering the material nonlinearity of anisotropic materials. The temporal shape, mode conversion effect, cumulative effect, and generation efficiency of QSP by GWs in composite pipes are investigated. For regional microscale damage in composite pipes, a simplified material model with microdamage is represented by variations of third-order elastic constants (TOECs) and incorporated in the time-domain 3D FE analysis. The proposed microdamage assessment method based on the measure of QSP is then discussed and compared with the experimental results measured in thermal fatigue damaged carbon fiber reinforced polymer (CFRP) pipes.

The paper is structured as follows. Section 2 describes the theoretical generation mechanism of QSP by longitudinal and transverse waves in anisotropic materials with weak quadratic material nonlinearity. In Section 3, a CFRP layered pipe is numerically analyzed regarding the dispersion and mode shape of GWs using the SAFE method. The time-domain 3D FE model for analyzing NGW propagation is also described. Section 4 shows the FE results and discusses the features of QSP in composite pipes. In Section 5, experiments are carried out using CFRP pipes, piezoelectric transducer array, and 3D laser vibrometer system. The results are analyzed and compared with FE data. Conclusions are drawn in Section 6.

2. Mechanism of quasistatic pulse generation

In general, FRP materials have polymer as a matrix and fiber as a strengthening substance. They are widely produced by stacking multiple layers to achieve the desired mechanical properties. A single layer, which consists of unidirectional fiber, can be regarded as transversely isotropic material. From a theoretical point of view, the material nonlinearity of such unidirectional FRP material can be expressed by the strain energy function that includes the strain terms up to third order as reported in [21,26]:

$$\begin{aligned} W = {} & \alpha_1(tr\mathbf{E})^2 + \alpha_2(tr\mathbf{E})(\mathbf{a}\cdot\mathbf{Ea}) + \alpha_3\left(tr\mathbf{E}^2\right) + \alpha_4(\mathbf{a}\cdot\mathbf{Ea})^2 + \alpha_5\left(\mathbf{a}\cdot\mathbf{E}^2\mathbf{a}\right) \\ & + \beta_1(tr\mathbf{E})^3 + \beta_2(tr\mathbf{E})\left(tr\mathbf{E}^2\right) + \beta_3(tr\mathbf{E})(\mathbf{a}\cdot\mathbf{Ea})^2 \\ & + \beta_4(tr\mathbf{E})\left(\mathbf{a}\cdot\mathbf{E}^2\mathbf{a}\right) + \beta_5(tr\mathbf{E})^2(\mathbf{a}\cdot\mathbf{Ea}) + \beta_6\left(tr\mathbf{E}^2\right)(\mathbf{a}\cdot\mathbf{Ea}) \\ & + \beta_7\left(tr\mathbf{E}^3\right) + \beta_8(\mathbf{a}\cdot\mathbf{Ea})^3 + \beta_9(\mathbf{a}\cdot\mathbf{Ea})\left(\mathbf{a}\cdot\mathbf{E}^2\mathbf{a}\right) + O\left(\mathbf{E}^4\right), \end{aligned} \tag{1}$$

Where $\mathbf{E}$ is the strain tensor, $\alpha_1 \sim \alpha_5$ are the linear elastic coefficients, $\beta_1 \sim \beta_9$ are the nonlinear elastic coefficients, $\mathbf{a}$ is the fiber direction unit vector. Assuming a Cartesian coordinate system (x_1, x_2, x_3), the primary wave propagates along the x_1 direction. The second Piola-Kirchhoof stress $\mathbf{S}$ is expressed by $\mathbf{S} = \partial W/\partial \mathbf{E}$, and the first Piola-Kirchhoff stress tensor is expressed by $\mathbf{P}(\mathbf{H}) = (\mathbf{I} + \mathbf{H})\mathbf{S}(\mathbf{H})$, where $\mathbf{I}$ is the identity tensor, and $\mathbf{H}$ is the displacement gradient tensor. Based on the balance of linear momentum $\mathbf{Div}(\mathbf{P}(\mathbf{H})) = \rho\ddot{\mathbf{u}}$, we can obtain the following results from five independent representative cases:

(i) For longitudinal wave $\mathbf{u} = (u_1^{\mathrm{L}}, 0, 0)$ propagating along the fiber direction $\mathbf{a} = (1, 0, 0)$, the nonlinear wave equation can be written as

$$\rho\ddot{u}_1 - A\frac{\partial^2 u_1}{\partial x_1^2} = B\frac{\partial u_1}{\partial x_1}\frac{\partial^2 u_1}{\partial x_1^2}, \tag{2}$$

where

$$\begin{aligned} A &= 2\alpha_1 + 2\alpha_2 + 2\alpha_3 + 2\alpha_4 + 2\alpha_5, \\ B &= 6\alpha_1 + 6\alpha_2 + 6\alpha_3 + 6\alpha_4 + 6\alpha_5 + 6\beta_1 + 3\beta_2 + 6\beta_3 + 4\beta_4 + 6\beta_5 + \frac{11}{2}\beta_6 + 6\beta_7 + 6\beta_8 + 6\beta_9. \end{aligned} \tag{3}$$

For $|BU^2k^2x_1/A| \ll 1$ and assuming the linear wave field as $u_1^{\mathrm{L}} = U\exp[j(kx - \omega t)]$ (U is the amplitude of primary wave, k is the wavenumber, and ω is the angular frequency), by using the perturbation technique, the solution to the Eq. (2) under the consistency condition [17] can be written as

$$u_1 = U\sin\left[\omega\left(t - \frac{x_1}{c_L}\right)\right] - \frac{BU^2\omega^2\rho}{8A^2}x_1 - \frac{BU^2\omega^2\rho}{8A^2}x_1\cos\left[2\omega\left(t - \frac{x_1}{c_L}\right)\right], \tag{4}$$

where c_L is the longitudinal wave velocity and ρ is the mass density. Here we can find the term $-BU^2\omega^2\rho x_1/8A^2$ represents the static strain caused by material nonlinearity and polarized in the wave propagation x_1 direction. It is noted that the coefficient A in Eq. (2) is a combination of second order elastic constants, and B indicates a combination of both second order and third order elastic constants. In practical applications, tone-burst ultrasound is widely used, and the propagating static strain exhibits a finite temporal width, namely QSP. When the material nonlinearity increases, the coefficient B increases, and the generation efficiency of QSP increases accordingly.

(ii) For longitudinal wave $\mathbf{u} = (u_1^{\mathrm{L}}, 0, 0)$ propagating perpendicular to the fiber direction $\mathbf{a} = (0, 1, 0)$ or $\mathbf{a} = (0,0,1)$, the equation of motion keeps the form of Eq. (2), while the coefficients in Eq. (3) are changed to:

$$\begin{aligned} A &= 2\alpha_1 + 2\alpha_3, \\ B &= 6\alpha_1 + 6\alpha_3 + 6\beta_1 + 3\beta_2 + 6\beta_7. \end{aligned} \tag{5}$$

Similarly, the QSP can be calculated by the second order perturbation method and expressed as:

$$u_{QSP} = -\frac{BU^2\omega^2\rho}{8A^2}x_1. \tag{6}$$

(iii) For shear wave $\mathbf{u} = (0, u_2^{\mathrm{L}}, 0)$ propagating along the fiber direction $\mathbf{a} = (1,0,0)$, the linear part of wave field can be written as

$$\rho\ddot{u}_2^{\mathrm{L}} - A\frac{\partial^2 u_2^{\mathrm{L}}}{\partial x_1^2} = 0, \tag{7}$$

where $A = \alpha_3 + \alpha_5/2$. For the nonlinear part of the wave field, the nonlinear term of the wave equation exists in the x_1 direction and can be expressed as

$$B\frac{\partial u_2^{\mathrm{L}}}{\partial x_1}\frac{\partial^2 u_2^{\mathrm{L}}}{\partial x_1^2} = \rho\ddot{u}_1, \tag{8}$$

where

$$B = 2\alpha_1 + 2\alpha_2 + 2\alpha_3 + 2\alpha_4 + 2\alpha_5 + \beta_2 + \frac{\beta_4}{2} + \beta_6 + \frac{3\beta_7}{2} + \frac{\beta_9}{2}. \tag{9}$$

It should be noted that the nonlinear term can act as the second order bulk driving force, which eventually leads to the generation of a static displacement polarized in the wave propagation x_1 direction.

(iv) For shear wave $\mathbf{u} = (0, u_2^{\mathrm{L}}, 0)$ propagating perpendicular to the fiber direction $\mathbf{a} = (0, 1, 0)$, the linear part of the wave field keeps the form of Eq. (7), and the coefficient A remains $A = \alpha_3 + \alpha_5/2$. For the nonlinear part of the wave field, the nonlinear term of

the wave equation exists in the x_1 direction and keeps the form of Eq. (8), while the coefficient B changes into

$$B = 2\alpha_1 + 2\alpha_3 + \beta_2 + \frac{\beta_4}{2} + \frac{3\beta_7}{2}. \tag{10}$$

(v) For shear wave $\mathbf{u} = (0, u_2^{\mathrm{L}}, 0)$ propagating perpendicular to the fiber direction $\mathbf{a} = (0,0,1)$, the linear part of wave field keeps the form of Eq. (7), while the coefficient A changes into $A = \alpha_3$. For the nonlinear part of the wave field, the nonlinear term of the wave equation exists in the x_1 direction and keeps the form of Eq. (8), while the coefficient B changes into

$$B = 2\alpha_1 + 2\alpha_3 + \beta_2 + \frac{3\beta_7}{2}. \tag{11}$$

It should be noted that there are three more cases, in which the combination of shear wave displacement direction and the fiber direction, results in the equivalent wave equations as in the case of (iii), (iv), and (v). Table 1 summarizes the above theoretical analysis. The significant feature of QSP is that its main displacement direction is always identical to the primary wave propagation direction. This feature remains true when it comes to GW propagation in anisotropic composites, as GW can be regarded as the superposition of a series of bulk waves. During the primary GW propagation, the QSPs generated by all the bulk wave components interfere with each other under the boundary conditions, and eventually form into one nonlinear signal with its displacement polarized in the propagation direction of the primary wave. Besides, the magnitude of QSP is partly dependent on the nonlinear elastic constants $\beta_1 \sim \beta_9$. With the increase of material nonlinearity, the magnitude of QSP increases as well. Moreover, the generation of QSP by material nonlinearity is independent of the synchronism condition and non-zero power flux condition as required by the cumulative generation of higher harmonics and wave mixing combined harmonics [20]. The inherent cumulative effect of QSP exhibits in the increases of amplitude when its group velocity matches the primary tone-burst wave and exhibits in the increases of temporal width when its group velocity is different from that of the primary tone-burst wave [20,21].

3. Numerical analysis

3.1. Determination of dispersion & mode shapes using SAFE method

Without loss of generality, in the subsequent numerical investigations, an analysis is conducted on a 2 mm thick CFRP pipe that comprises both circumferential and axial fibers. The inner radius of the composite pipe is 48 mm, and the outer radius is 50 mm. The CFRP pipe is constructed by stacking 10 layers of ply, as illustrated in Fig. 1. Due to the anisotropy of such material, the properties of GW propagation regarding the dispersion feature and mode shapes are calculated by the SAFE method [25]. The mechanical properties of a single unidirectional layer of the CFRP pipe and its mass density are listed in Table 2. The eigenvalue problem in the frequency domain is then solved by considering both the analytical expression along the waveguided and the FE discretization imposed on the section of the waveguide. Fig. 2 shows the phase velocity and group velocity dispersion curves. Fig. 3 shows the mode shapes (i.e., wave structures) of the three lowest order axisymmetric GW modes at 200 kHz propagating in the CFRP pipe. In Fig. 3, the black arrows indicate the displacement component in the cross-section plane (XY plane in Fig. 1), and the color maps indicate the displacement component in the Z direction (wave propagation direction). As shown in Fig. 3(b), the T(0,1) wave mode has only torsional displacement polarized in the XY plane. Comparing Fig. 3(a) and (c), the L(0,2) has greater Z-displacement than the L(0,1) wave mode. This characteristic of longitudinal modes is in line with the mode shapes of GWs in isotropic metallic pipes [27]. The GW modal

Table 1
QSP generation of ultrasonic waves with different configurations in transversely isotropic materials. The primary wave propagates along x_1 direction.

Configuration Displacement direction of primary wave Fiber direction	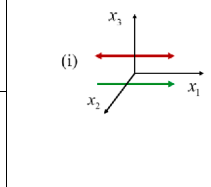	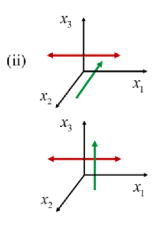	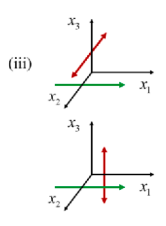	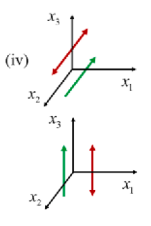	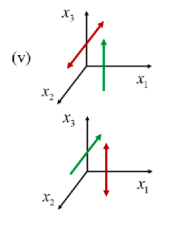
Displacement direction of QSP	Primary L wave propagation x_1 direction	Primary L wave propagation x_1 direction	Primary S wave propagation x_1 direction	Primary S wave propagation x_1 direction	Primary S wave propagation x_1 direction
A (ρc^2)	$2\alpha_1 + 2\alpha_2 + 2\alpha_3 + 2\alpha_4 + 2\alpha_5$	$2\alpha_1 + 2\alpha_3$	$\alpha_3 + \alpha_5/2$	$\alpha_3 + \alpha_5/2$	α_3
B	$6\alpha_1 + 6\alpha_2 + 6\alpha_3 + 6\alpha_4 + 6\alpha_5 + 6\beta_1 + 3\beta_2 + 6\beta_3 + 4\beta_4 + 6\beta_5 + \frac{11}{2}\beta_6 + 6\beta_7 + 6\beta_8 + 6\beta_9$	$6\alpha_1 + 6\alpha_3 + 6\beta_1 + 3\beta_2 + 6\beta_7$	$2\alpha_1 + 2\alpha_2 + 2\alpha_3 + 2\alpha_4 + 2\alpha_5 + \beta_2 + \frac{\beta_4}{2} + \beta_6 + \frac{3\beta_7}{2} + \frac{\beta_9}{2}$	$2\alpha_1 + 2\alpha_3 + \beta_2 + \frac{\beta_4}{2} + \frac{3\beta_7}{2}$	$2\alpha_1 + 2\alpha_3 + \beta_2 + \frac{3\beta_7}{2}$

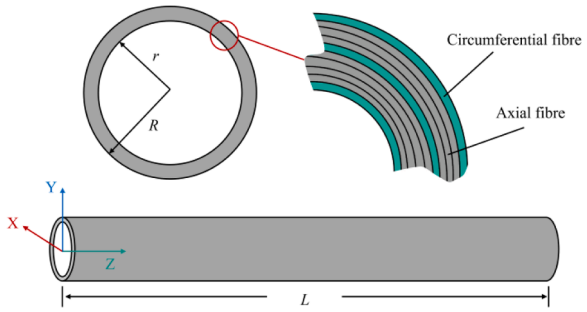

Fig. 1. Schematic of CFRP pipe with stacking order [C/A_4/C/A_3/C] (C: circumferential fiber, A: axial fiber), inner radius $r = 48$ mm, outer radius $R = 50$ mm.

Table 2
Second order stiffness constants (Unit: GPa) and mass density (kg/m^3) of a single CFPR layer used in numerical analysis.

C_{11}	C_{12}	C_{13}	C_{22}	C_{23}	C_{33}	C_{44}	C_{55}	C_{66}	Density
143.8	6.2	6.2	13.3	6.5	13.3	3.4	5.7	5.7	1560

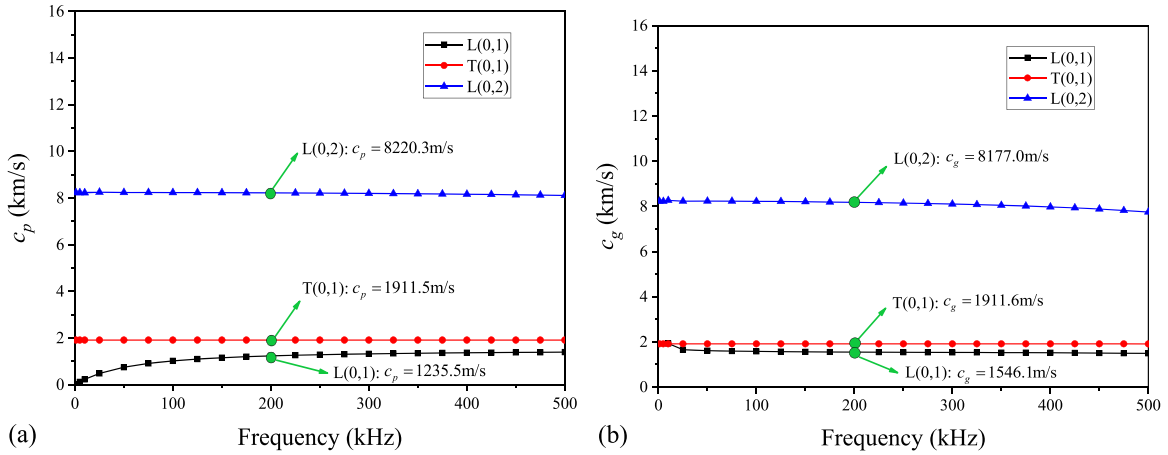

Fig. 2. Dispersion curves of GWs: (a) phase velocity, (b) group velocity.

analysis of such composite structure provides guidance for effective wave excitation and receiving in the following 3D time domain simulation and experiments.

3.2. FE modelling of GW propagation

To verify the wave modal analysis in Section 3.1, time domain modelling and simulation are conducted. The three lowest order of axisymmetric GW modes are in turn employed as primary wave for the wave propagation simulation using a 3D FE model developed in Abaqus/CAE Explicit. Fig. 4 shows the schematic of the FE model. For tone-burst GW excitation, the left end surface is loaded with a user-defined displacement function. The displacement is a Hann windowed sinusoidal wave with its frequency, cycle, and maximum amplitude respectively denoted as f, N, and $U_{\max}$ (excitation: $f = 200$ kHz, $N = 10$, $U_{\max} = 100$nm; receiving: $\theta = 0°$). For ease of signal interpretation, a cylindrical coordinate system ($r - \theta - z$) is used with the origin is located at the center of the left end face (i.e., $r - \theta$ plane) and the z direction is in line with the global X-Y-Z coordinate system. According to the mode shapes shown in Fig. 3, the displacement functions for the three primary wave modes are respectively prescribed in r, θ, and z directions as shown in Fig. 4. This is to ensure that a relatively pure mode can be introduced into the pipe for each simulation, which facilitates the signal analysis. For receiving the signal, several measuring points are set at $Z = L$ surrounding the outer surface of the composite pipe. The geometry is meshed with structured hex elements of type C3D8R. Referring to [28], the maximum mesh size of the model is determined by $\Delta_m \leq \lambda/20$ (λ is the wavelength of the primary wave). The time step of the transient response study is determined by $\Delta_t \leq 1/20f$ (f is the wavelength of the primary wave). The convergence of the model is confirmed by the fact that the wave velocity and amplitude of the primary GW barely change when further decreasing the mesh size and time step.

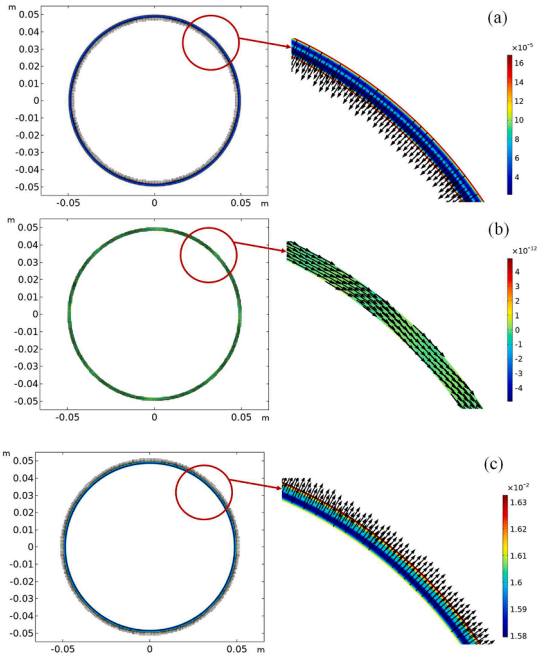

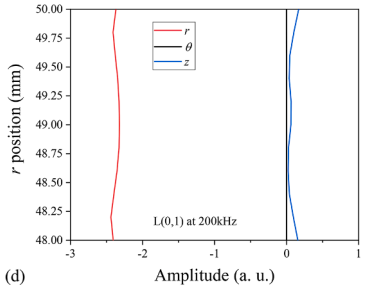

(d)

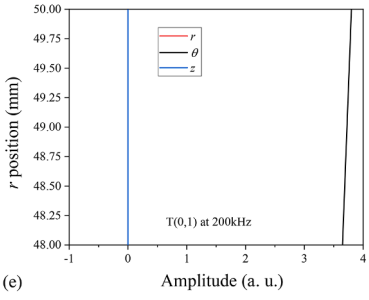

(e)

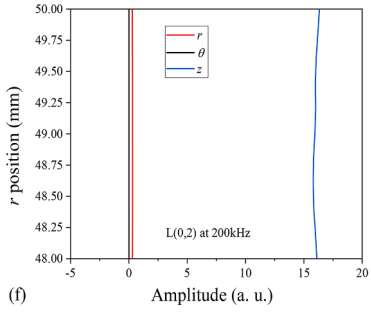

(f)

(caption on next page)

Fig. 3. Mode shapes of GWs at 200kHz: (a) L(0,1) mode, (b) T(0,1) mode, (c) L(0,2) mode. Black arrows indicate the displacement component in the cross-section plane, and color maps indicate the displacement component in the wave propagation direction; wave structures of (d) L(0,1) mode, (e) T(0,1) mode, (f) L(0,2) mode at 200 kHz.

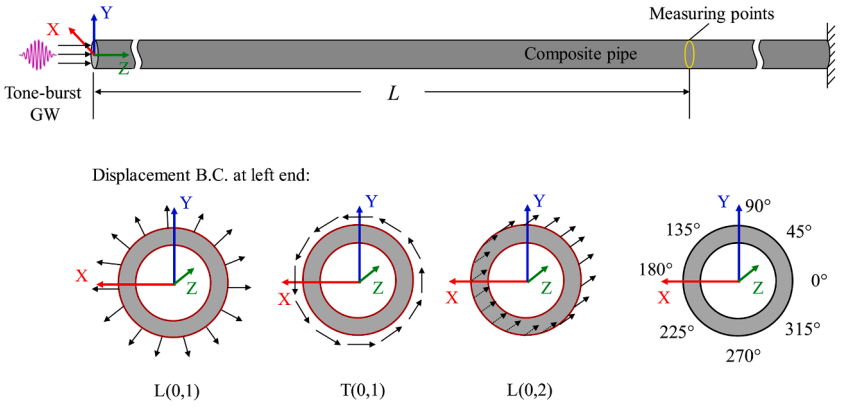

Fig. 4. Illustrations of FE models for simulation of time domain wave propagation.

To analyze the QSP generation induced by material nonlinearity, the third order elastic stiffness constants of the composite pipe are introduced into the simulation using a user-defined subroutine that customized the material constitutive model. Based on Section 2.1, the nonlinear elastic coefficients of $\beta_1 \sim \beta_9$ are related to the nine independent third order stiffness constants of a single CFRP layer [21], which are shown in Table 3. Besides, the regional micro-damage is modelled by scaling up ξ_N times the third order stiffness constants. Given the complexity of the microscale properties inherent in CFRP materials, this method serves as a highly effective approximation for detecting the presence of microdamage, as it elicits discernible nonlinear responses.

As a pre-validation of the 3D time domain model, Fig. 5 shows the typical temporal signals of the primary L(0,1), T(0,1), and L(0,2) modes received at $Z = 0.25$ m, 0.50 m, and 0.75 m. The group velocities of these three primary modes are calculated as 1612.8 m/s, 1995.6 m/s, and 8011.3 m/s, respectively. These values of group velocity are consistent with the theoretical dispersion curves shown in Fig. 2 with less than 5 % errors. Besides, the main displacements of these three modes are polarized in the *r*, θ and *z* directions. This is also in line with the theoretically predicted mode shapes shown in Fig. 3.

4. Features of quasistatic pulse in composite pipes

4.1. Mode conversion and cumulative effect

The observation of QSP in the CFRP pipe with quadratic material nonlinearity is achieved using the phase reversal method [29,30], as the QSP displacements are nonlinear signals and have similar properties to the even harmonics. Fig. 6 shows the temporal QSP signals generated from the propagations of the primary modes of L(0,1), T(0,1), and L(0,2). The primary waves at 200 kHz are presented in Fig. 5. The displacements detected in *Z* direction of two primary waves of opposite phases are superposed and denoted by $U_z^{'}$. As shown in Fig. 6(a)–(c), the three generated QSP signals have almost the same pulse velocity $c \approx 8200$ m/s of L(0,2) mode. Besides, the displacement of QSP is mostly polarized in Z direction. This indicates that different fundamental GWs can generate the QSP of L(0, 2) mode in the anisotropic CFRP pipes considering the material nonlinearity.

Besides, the effect of group velocity mismatching is also observed in Fig. 6(a) and (b). Due to the difference in velocity between the primary L(0,1)/T(0,1) mode and the corresponding QSP of L(0,2) mode, the pulse width of QSP starts increasing shortly after its amplitude increases to a certain degree. The leading edge of the QSP signal has the velocity of L(0,2) mode, and the ending edge has the velocity of the corresponding primary mode. Since the shape of the ending part of the QSP signal is related to the displacement excitation condition in the FE simulation [17], we can focus on the leading part of the QSP signal in the following analysis. Specifically, when the primary mode is L(0,2) mode, the generated QSP can propagate along with the primary wave and only its amplitude increases with propagation distance as shown in Fig. 6(c). This feature of QSP generation on the condition of group velocity matching is significantly useful for microdamage detection in a large area, as the cumulative increase of displacement amplitude of QSP can readily indicate the level of material nonlinearity of materials.

Table 3
Third order stiffness constants (Unit: GPa) of a single CFPR layer used in numerical analysis [26].

C_{111}	C_{112}	C_{155}	C_{222}	C_{223}	C_{122}	C_{123}	C_{255}	C_{266}
1000	65	−47	−214	−89	−4	65	−33.4	−49.1

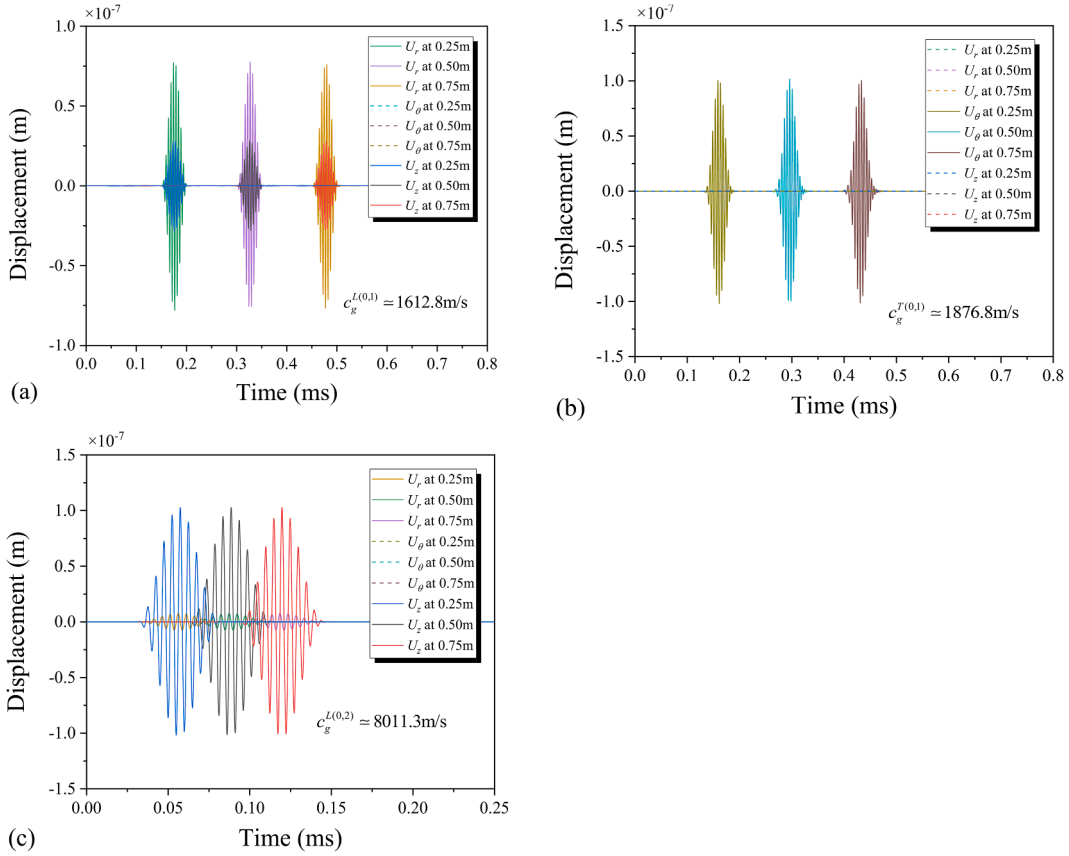

Fig. 5. Time domain signals of primary modes: (a) L(0,1), (b) T(0,1), (c) L(0,2). The modes are consistent with the theoretical dispersion curves regarding their group velocities.

4.2. Generation efficiency

Since the wave structures of different primary modes are different, and there are nine independent third order elastic constants in a single unidirectional FRP composite layer, the generation efficiency of QSP can vary with the primary modes and many other factors. Based on the time-domain accumulation feature of QSP and for consistency of comparison, the integration of QSP amplitude over time ($|\int U_z|$) is employed as an index of generation efficiency of QSP by all primary modes. The integration interval is defined as between two time points of the QSP with zero displacement amplitudes at the nearest left and right sides of the pulse. As shown in Fig. 7(a), the generation efficiency of QSP in terms of the amplitude of primary waves is ranked as: L(0,1)>L(0,2)>T(0,1). Similarly, by keeping the amplitude of primary waves at the same level as 100 nm, the generation efficiency of QSP regarding the propagation distance is also ranked as: L(0,1)>L(0,2)>T(0,1) (See Fig. 7(b)). However, the interferences between the different effects of the third order elastic constants on the QSP generation result in the opposite trend of QSP generation in terms of the scaling coefficient ξ_N of third order elastic constants. As shown in Fig. 7(c), the QSP generation of primary L(0,1) and T(0,1) waves decreases when increasing all the third order elastic constants, while the generation efficiency increases for L(0,2) primary wave. This indicates that the effective detection of material nonlinearity in FRP composite pipes using QSP generation is greatly dependent on the optimized combination of primary wave mode, excitation magnitude, and wave propagation distance.

4.3. Duration effect on QSP generation

Another important feature of QSP generation is that the number of cycles of the primary tone-burst GW can influence the absolute amplitude of QSP generated by the group velocity-mismatched primary wave. As shown in Fig. 8(a) and (b), while keeping the frequency and excitation magnitude of primary waves the same, the absolute amplitude of QSPs by L(0,1) and T(0,1) can increase with the number of cycles (i.e., tone-burst duration) of the primary GW. For the case of L(0,2) mode, since the cumulative effect of QSP only displays in the amplitude and not in the temporal width for group velocity matching, the increase of duration of primary GW can only lead to the increase of wave packet length rather than the amplitude of QSP. Fig. 8(c) shows the comparison of the duration effect on QSP generation in pipes across these three primary modes.

It should be noted that, in the FE simulation, GW propagations of different single primary modes are modeled and analyzed

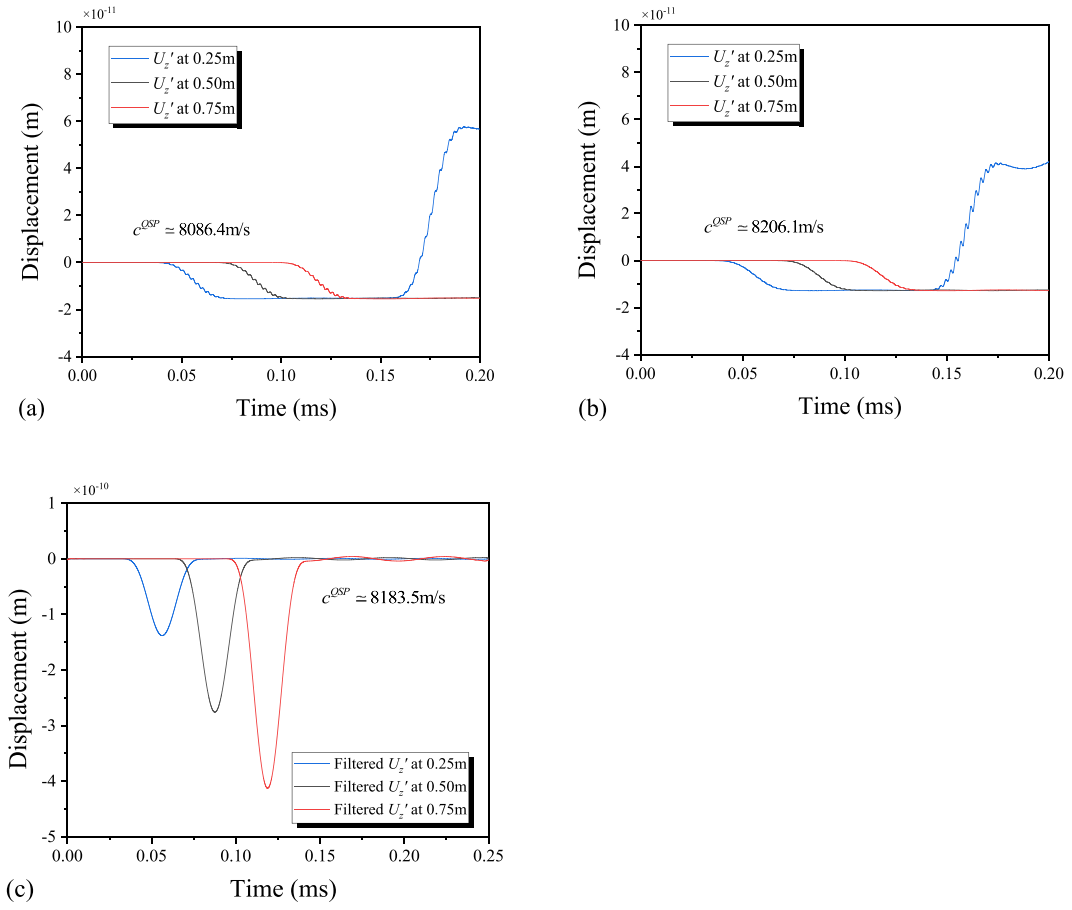

Fig. 6. Time domain signals of QSP generated by primary waves and processed by phase reversal method: (a) by L(0,1) mode, (b) by T(0,1) mode, (c) by L(0,2) mode.

regarding the QSP generation. This facilitates the demonstration of QSP generation and enhances the understanding of the physical mechanism. However, in practical applications, multimodal GWs can be readily excited into the pipe-like waveguides due to different boundary conditions from the perfect mode shapes of the desired mode. For instance, the excitation of L(0,2) mode using a transducer array attached around the pipe inevitably introduces the L(0,1) mode into the pipes. However, based on the above analysis of QSP generation, it is indicated that the induced nonlinear QSPs can possess the same fastest group velocity among all the possible fundamental GW modes. Hence, in scenarios where multiple primary modes are present, the analysis of QSP primarily concentrates on the initial segment of the measured signal, which exhibits polarization in the axial Z direction.

5. Experiments

5.1. Specimens

The specimens used in the following experiments are commercially purchased CFRP pipes. The pipes comprise 10 unidirectional layers with a stacking order of [C/A_4/C/A_3/C] (C: circumferential fiber, A: axial fiber). The inner radius is 48 mm, the outer radius is 50 mm, and the length is 1.5 m. The total thickness of the pipes is 2 mm. The mass density of the pipe is 1560 kg/m^3. The properties of carbon fiber and epoxy resin as separated materials are listed in Tables 4 and 5, respectively. The pipe specimens were produced using carbon fiber and epoxy under high temperature and pressure in specialized equipment. For a unidirectional layer of such CFRP materials, the stiffness matrix components are around the values provided by the manufacturer and listed in Table 2.

For the feasibility study of microdamage assessment using QSP generation, artificial thermal fatigue damage was introduced into the CFRP pipes. A heat gun (BOSCH GHG 600–3) was set 30 mm upon the CFRP pipe with the heating temperature set as 300 °C . Regional thermal fatigue damage was incurred across the entire pipe by moving the heating point at regular intervals of 0.05 m along the pipe's length and rotation of 22.5° around its circumference for each specified processing time. The pipe was heated for 30 s at each fixed position, and the process was carried on for different times to compare the results of ultrasonic GW tests. Fig. 9 shows a picture of the CFPR pipes, heat gun, and illustration of the heating process. In the process of thermal cycling, composite laminates experience

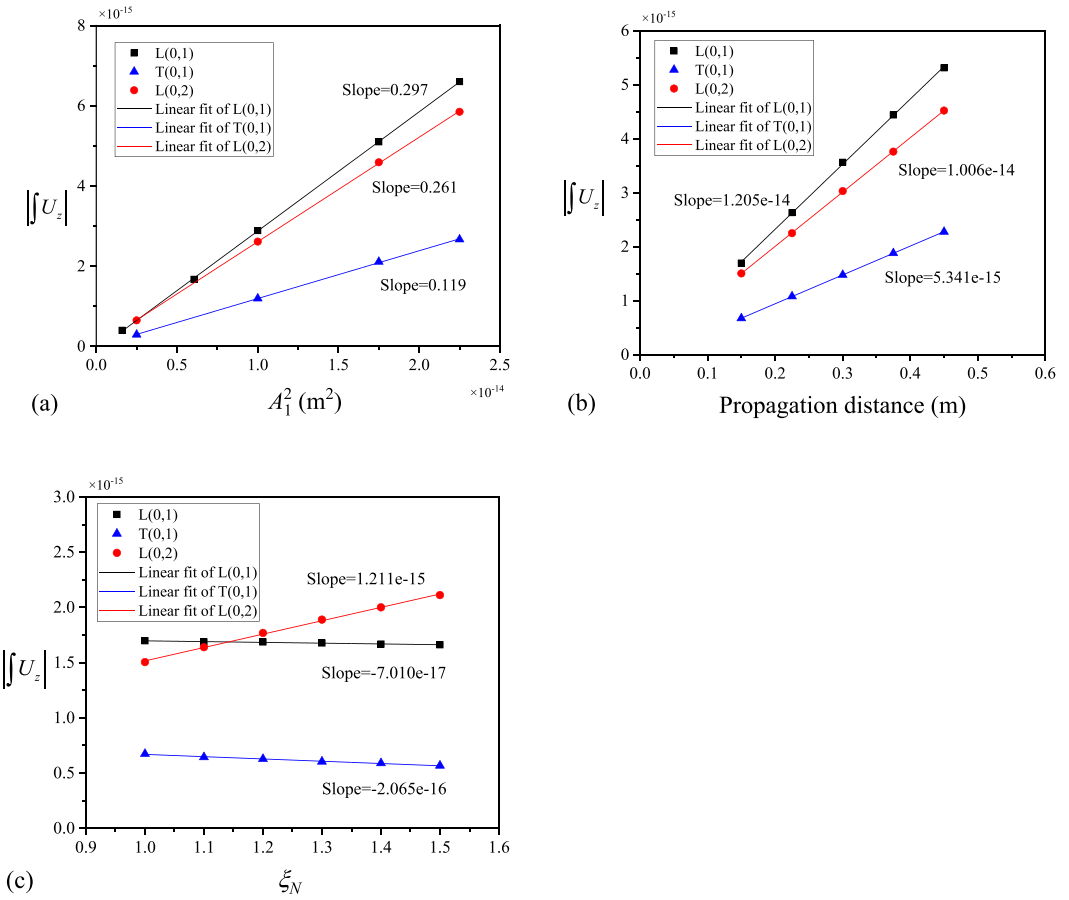

Fig. 7. Comparison of QSP generations in CFRP pipe: magnitude of QSP with respect to (a) amplitude of primary GW, (b) propagation distance, (c) magnification factor of nonlinear elastic constants.

thermal stresses. These recurring thermal stresses can lead to damage akin to what is seen under mechanical cyclic loading, including micro-scale damages in the forms of transverse matrix cracks, debonding, and delamination within the layers [31,32]. Consequently, the heating process degraded the fiber reinforced composites. From the nonlinear ultrasonic point of view, these micro-scale changes inside the materials are intrinsically related to the variations of elasticity properties of the materials, which can be characterized by the measurement of higher order elastic constants [33]. Thus, the QSP generation of guided waves, as one of the nonlinear ultrasonic responses, can also be potentially used for the evaluation of micro-damages in composite materials.

5.2. Experimental setup

The ultrasonic excitation and measurements were conducted using the NI signal generator, high-power amplifier, piezoceramic transducer, and 3D laser Doppler scanning vibrometer system (LDV, Polytech PSV-400). Fig. 10 shows the schematic diagram and pictures of the experiment setup. The Hann windowed tone-burst sinusoidal signal was customized and generated by the NI signal generator (PXIe-5122). After being amplified by the high-power amplifier (CIPRIAN HVA-800A), the high-voltage signal was transmitted to the shear piezoceramic transducers (Dimensions: 10.0mm×5.0mm×2.0 mm). The transducers were evenly glued upon the outer surface of the CFRP pipe at one end using conductive epoxy (Chemtronics CW2400). The vibration mode of the piezoceramic actuators is mainly in shear direction (i.e., parallel to the axial direction of the pipes). As a result, the longitudinal L(0,2) mode can be introduced into the pipe at the largest efficiency. Ultrasonic GWs were excited into the pipe and propagated towards the other end of the pipe. The GWs were eventually picked up by the 3D laser Doppler vibrometer. To enhance the reflectivity of the laser beams, the measurement area of the CFRP pipe was painted with a reflective coating (CRC 18015). The recorded signals were averaged 1500 times to improve the signal-to-noise ratio. Digital low-pass filters were applied to the received signals by the data acquisition system. The same process at each testing location was repeated three times to minimize the measurement errors.

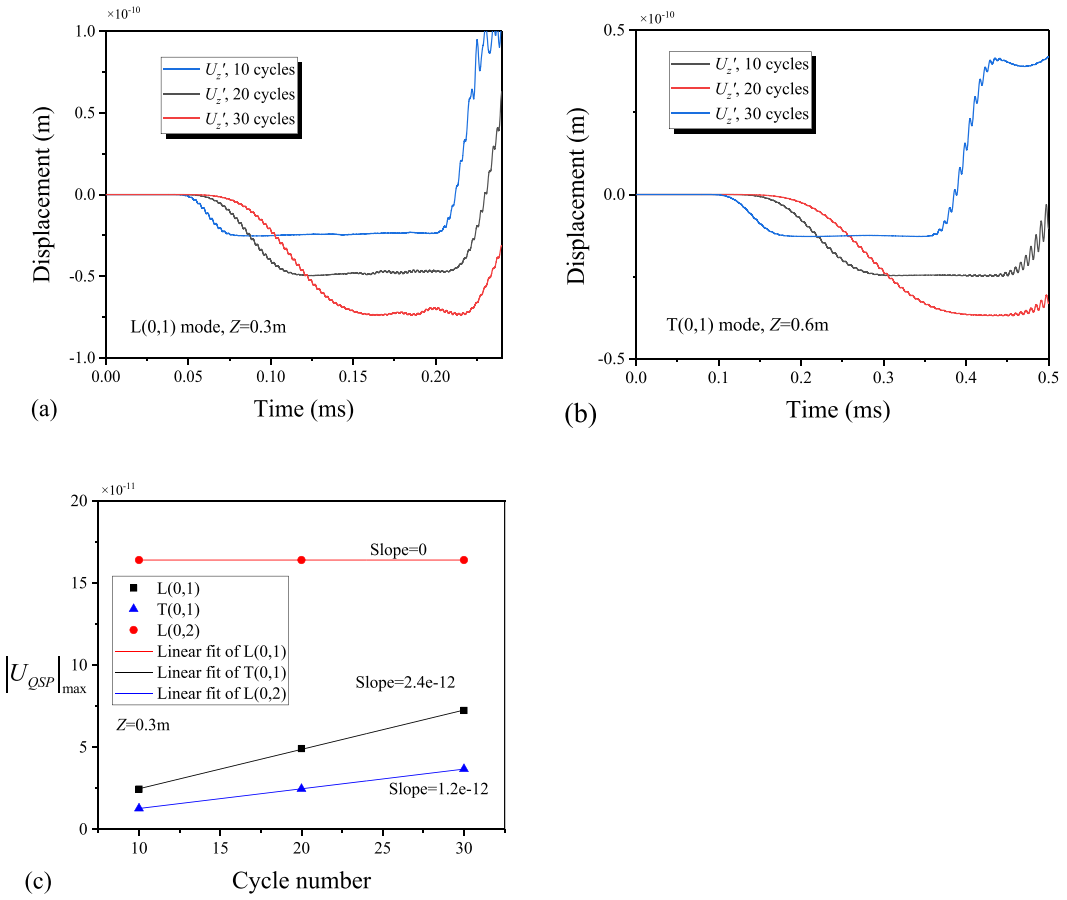

Fig. 8. Duration effect of primary wave on the amplitude of QSP: time-domain signals of QSPs generated by (a) L(0,1) mode and (b) T(0,1) mode of different tone-burst length, (c) comparison of different primary modes.

Table 4
Properties of carbon fiber.

Tensile modulus	Tensile strength	Elongation	Density
242 GPa	4550 MPa	1.8 %	1790 kg/m^3

Table 5
Properties of epoxy resin.

Vitrification transition temperature	Tensile modulus	Tensile strength	Bending modulus	Bending strength
125℃~135℃	3.82GPa	80MPa	4.28GPa	115MPa

5.3. Results & discussions

5.3.1. Analysis of primary waves

As discussed in Section 4.1 and shown in Fig. 6(c), the QSP generation exhibits cumulation in amplitude with propagation distance when the primary GW has the same group velocity as the induced QSP wave. Therefore, we expect that the L(0,2) mode is excited into the pipe by the eight shear piezoceramic transducers. Due to the similarity between the mode shape of L(0,2) mode and the setup of actuators, the excitability of L(0,2) mode is optimized. However, the transducer array can still result in the occurrence of multiple GW modes. While the primary GWs propagate along the axis of the pipe (Z direction), they also scatter away towards the circumferential direction of the pipe. Therefore, the multimodal feature and the interference of GWs from different wave sources lead to the oscillation of wave amplitude measured at different locations.

We first measured the primary waves in intact pipe specimen. As shown in Fig. 11(a), the out-of-plane displacements U_r of the 200

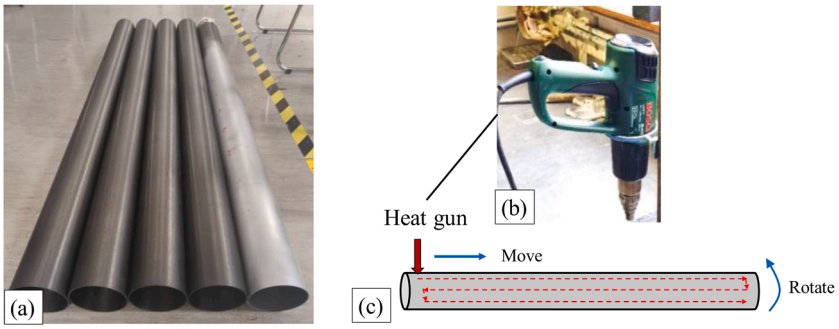

Fig. 9. (a) CFRP specimens, (b) Thermal gun used for heating CFRP specimens, (c) Illustration of heating process.

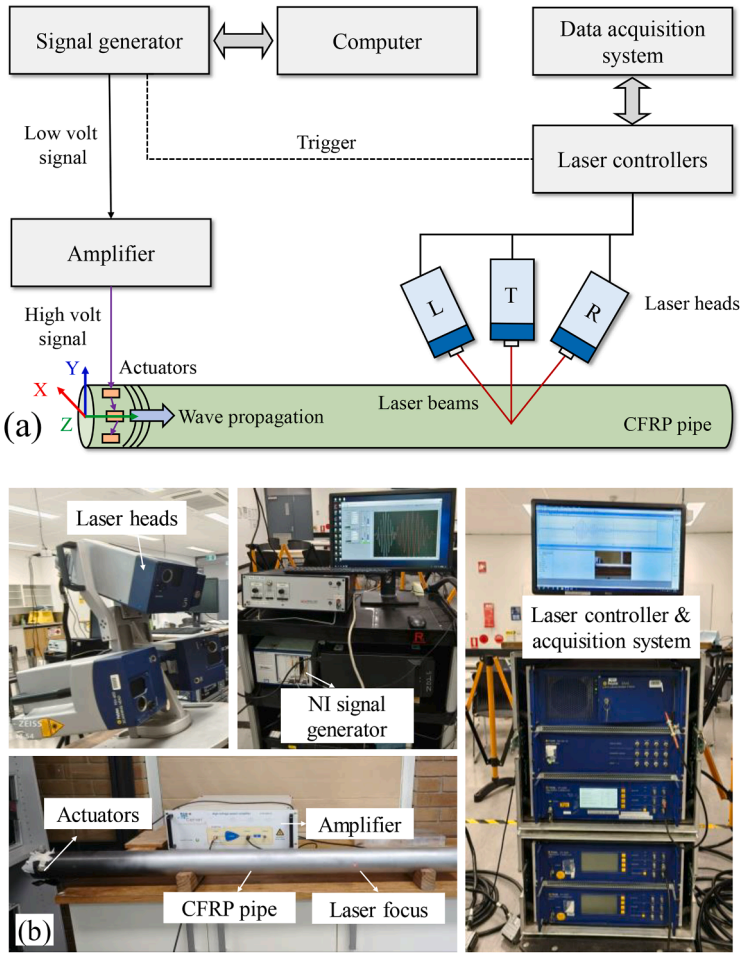

Fig. 10. Experimental setup: (a) schematic diagram, (b) physical pictures.

kHz primary waves at different axial locations are extracted. The group velocity of the fundamental wave packet is calculated as about 1610 m/s. Referring to the dispersion curves shown in Fig. 2, it is indicated that the L(0,1) mode is generated into the pipe. Besides, it should be noted that the out-of-plane amplitudes of L(0,1) mode measured at different locations do not decrease with the propagation distance. This oscillation of amplitude is due to the interference of waves from the transducer array. On the other hand, the axial displacements of the primary waves are extracted and shown in Fig. 11(b). The first wave packet has a group velocity of around 8026 m/s, which is in line with the L(0,2) mode at 200 kHz. There are many other primary wave packets polarized in the axial direction. In comparison to Fig. 6(c), which is obtained by exciting pure L(0,2) mode into the pipe, this is the experimental phenomenon that multiple GW modes are introduced into the pipe.

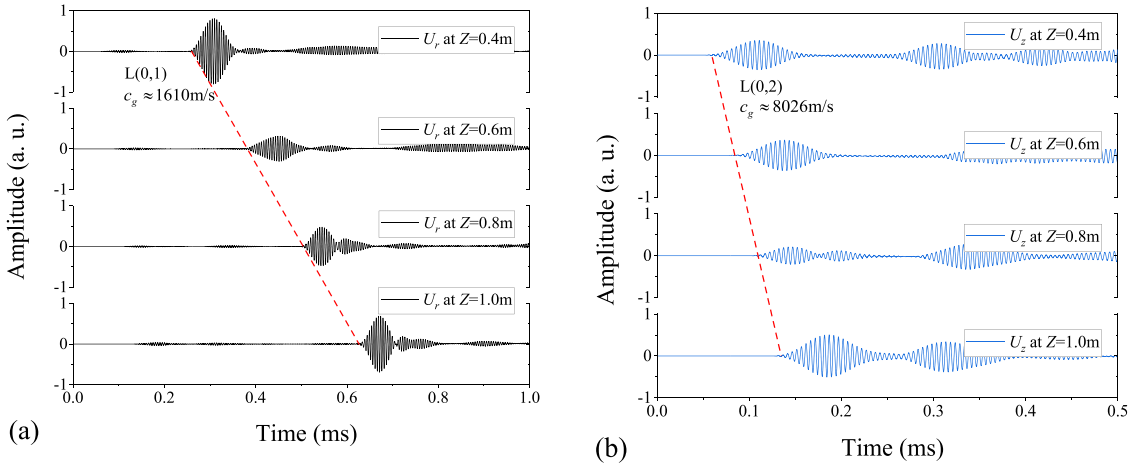

Fig. 11. Fundamental waves received in the (a) r direction and in the (b) z direction at different propagation distances.

5.3.2. *Identification of QSP generation*

To extract the QSP signals, the phase reversal method [34] was used. As the QSP is one of the even nonlinear responses of GW propagation, it can be amplified by two times when superposing the two received wave fields of opposite excitation phases [17]. In the meantime, the offset of two fundamental waves will occur. This method can significantly enhance the signal-to-noise ratio for the QSP measurement. Besides, the measured signals were averaged 1500 times and digital filtered. The axial displacements, which are generated by primary waves of the opposite phase, are measured at the different locations along the Z direction of the pipe. For a specific measurement location, the two axial signals are superposed and low pass filtered. The cut-off frequency of the digital filter is set as the main frequency of primary waves.

Fig. 12 shows the QSP signals measured at different Z locations at $\theta = 0^{\circ}$. Based on the analysis of QSP by FE simulation results in Section 4, we infer that the QSP signal is formed by the superposition of many QSP components of different primary GW modes. The QSPs generated by all primary waves possess the same largest possible group velocity of GWs in the pipe. Since there exists a series of primary wave packets in the axial direction, it can be compared with the circumstance that a primary wave with a long duration is excited. As shown in Fig. 8, the duration effect can lead to the amplitude increase of QSP for group velocity-mismatched mode pairs. Thus, in the experiment, the constructive interference of QSP components eventually leads to the increase of its amplitude to a certain degree. This increase is not only due to the cumulative effect of QSP that is generated under the group velocity matching condition with the primary L(0,2) mode, but also due to the duration effect provided by the other multiple relatively slower primary GW modes. The group velocity of the resultant QSP signal is calculated as about 8071 m/s, which is consistent with the dispersion curves of L(0,2) mode at zero frequency. This verifies the theoretical and FE simulation analyses. It is noted that the QSP signal does not increase with the propagation distance in the experiment. This is because the primary wave packets are subject to dispersion, attenuation, and interference with each other. Unlike a pure fundamental GW mode that can be simulated in FE modeling, the primary GW signals measured at different axial and circumferential locations have different magnitudes in practice.

To further validate the QSP generation and propose a feasible nonlinear parameter for microdamage detection in composite pipes, different excitation levels and frequencies of primary GWs are induced into the pipe. As the out-of-plane displacement signal U_r has obviously fewer wave packets than that extracted in the axial in-plane direction, the relation of the absolute magnitude of QSP signals $|U_{QSP}|_{\max}$ against the square of the out-of-plane displacement U_r^2 is presented in Fig. 13. It is found that there is a linear relationship between the magnitude of QSP signal and the square of primary GW magnitude. Moreover, when increasing the frequency of primary waves, the slope of its linear fit increases significantly as well. These results are consistent with the theoretical and numerical studies. For a single primary wave mode, the squares of magnitude and frequency of the primary wave are theoretically linear and proportional to the generation efficiency of the corresponding nonlinear QSP signal. In the experiment, although the generated primary wave is multimodal, the relationship between the extracted QSP amplitude and the primary out-of-plane displacement shows similar effects of the excitation magnitude and frequency of the primary wave on the QSP generation.

5.3.3. *Microdamage assessment using QSP*

Based on the analysis in the above section, the relative nonlinear acoustic parameter employing the QSP generation is constructed as

$$\widetilde{\beta}_{QSP} = \frac{|U_{QSP}|_{\max}}{U_r^2}. \tag{12}$$

The ultrasonic signals are in turn measured in three CFRP pipes (#1, #2, #3) using the same process. By repeating the heating cycle of the pipe for different times, the early-stage thermal fatigue microdamage is generated in the pipes. The measurement point is set as $Z = 1.0$ m and $\alpha = 0^{\circ}$. After acquiring the GW signals, the wave velocities of primary modes are calculated to be nearly the same, which

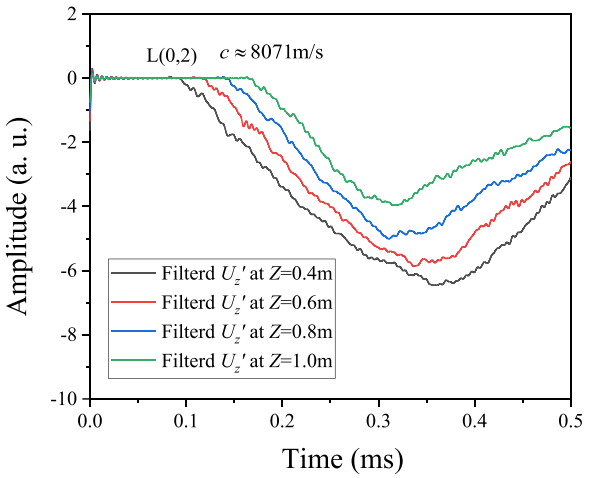

Fig. 12. Low pass filtered QSP signals received at different axial Z locations.

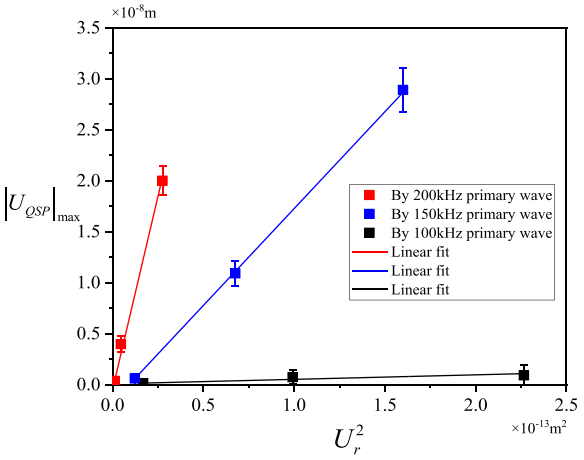

Fig. 13. Relationship of absolute magnitude of QSP signals against that of primary waves.

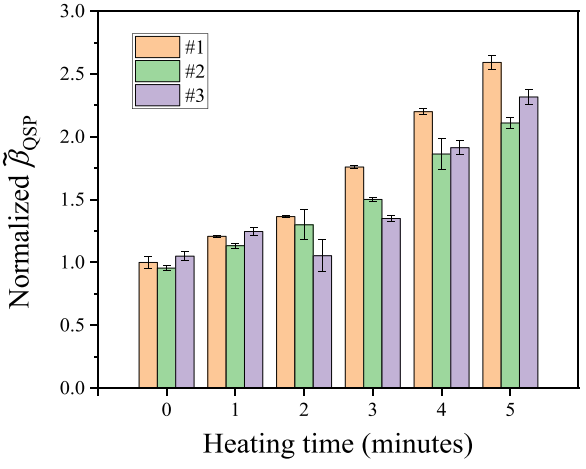

Fig. 14. Measured relative nonlinear acoustic parameter $\tilde{\beta}_{QSP}$ with respect to the total heating time of CFRP pipes.

suggests the ineffectiveness of linear ultrasound techniques using wave velocity. On the other hand, the comparison of the proposed parameter $\widetilde{\beta}_{QSP}$ of the three CFRP pipes is shown in Fig. 14. The calculated $\widetilde{\beta}_{QSP}$ is found to increase with the total heating time for pipes #1 and #2, while a slight decrease occurs for pipe #3 when the heating time is 2 min. This may be due to the inconsistency of the microdamage in the specimens. However, the overall trend of the variation of $\widetilde{\beta}_{QSP}$ indicates that this proposed nonlinear ultrasonic index is sensitive to thermal fatigue damage in CFRP composite pipes.

It should be noted that, under the current experimental conditions, we cannot yet achieve the perfect excitation of a pure L(0,2) mode inside the pipe specimens. For practical microdamage evaluation, the measurement of QSP signals using the identical experimental setups for different specimens is required for effectively comparing the variations of material properties. However, the generated QSP waves by different primary GW modes propagation in pipe have the same pulse velocity and are always the fastest longitudinal mode. Although both the primary wave and the generated QSP wave are influenced by the excitation condition, this unique feature of QSP generated by GWs in pipe makes the mode recognition of QSP wave less troublesome. Besides, the energy of generated QSP is less dissipated in cylindrical shell than in plate structures, and QSP suffers little the acoustic attenuation in composites as well. Thus, this generated QSP signal can be more readily predicted and analyzed than higher harmonic waves in a certain degree.

6. Conclusions

This study presents the numerical and experimental investigations on the quasistatic pulse generation in CFRP composite pipes. The theoretical background of QSP generation in anisotropic materials has been demonstrated and summarized. Features including the temporal waveform, cumulative effect, generation efficiency, and duration effect of the QSP generated by different primary guided wave modes have been studied by FE modeling and simulation. Experimental observations of the nonlinear QSP signals measured in CFRP pipes have been conducted using piezoceramic transducer array and the 3D laser vibrometer scanning system. The absolute amplitude of the QSP signal has been found to be proportional to the excitation magnitude and frequency of the primary wave. The relative nonlinear acoustic parameter of the amplitude ratio $\widetilde{\beta}_{QSP}$ has been proposed. The results of $\widetilde{\beta}_{QSP}$ measured in CFRP pipes have shown high sensitivity to early-stage thermal fatigue damage in composite pipes compared to linear ultrasonic characteristics.

CRediT authorship contribution statement

Chang Jiang: Conceptualization, Methodology, Writing – original draft. **Weibin Li:** Supervision, Writing – review & editing. **Ching-Tai Ng:** Supervision, Writing – review & editing. **Mingxi Deng:** Supervision, Writing – review & editing.

Declaration of competing interest

The authors declare that they have no known competing financial interests or personal relationships that could have appeared to influence the work reported in this paper.

Data availability

Data will be made available on request.

Acknowledgments

This work was supported by the National Natural Science Foundation of China under grant nos. 11974295, 12134002, 11834008, and 12074050. Meanwhile it was also supported by the project of Basic Technology Research which is funded by Technology and Quality Division of the Ministry of Industry and Information Technology of China (grant no: JSZL2018602C001), the Principal Fund of Xiamen University (grant no: 20720210040), and the China Scholarship Council (no. 202006310008).

References

[1] F.G. Alabtah, E. Mahdi, F.F. Eliyan, The use of fiber reinforced polymeric composites in pipelines: a review, Compos. Struct. 276 (2021) 114595, https://doi.org/10.1016/j.compstruct.2021.114595.
[2] O. Ahmed, X. Wang, M.-V. Tran, M.-Z. Ismadi, Advancements in fiber-reinforced polymer composite materials damage detection methods: towards achieving energy-efficient SHM systems, Composit. Part B 223 (2021) 109136, https://doi.org/10.1016/j.compositesb.2021.109136.
[3] J.L. Rose, Y. Cho, M.J. Aviolis, Next generation guided wave health monitoring for long rangeinspection of pipes, J. Loss Prev. Process Ind. 22 (2009) 1010–1015, https://doi.org/10.1016/j.jlp.2009.08.011.
[4] R. Guan, Y. Lu, W. Duan, X. Wang, Guided waves for damage identification in pipeline structures, Areview. Struct Control Health Monit 24 (2017) e2007, https://doi.org/10.1002/stc.2007.
[5] Z. Su, L. Ye, Y. Lu, Guided Lamb waves for identification ofdamage in composite structures: a review, J. Sound Vib. 295 (2006) 753–780, https://doi.org/10.1016/j.jsv.2006.01.020.
[6] M.F. Hamilton, D.T. Blackstock, Nonlinear Acoustics, Academic Press Inc, San Diego, CA, 1998.
[7] K-Y Jhang, CJ Lissenden, I Solodov, Y Ohara, V Gusev (Eds.), Measurement of Nonlinear Ultrasonic Characteristics, Springer, Singapore, 2020.

[8] V.K. Chillara, C.J. Lissenden, Review of nonlinear ultrasonic guided wave nondestructive evaluation: theory, numerics, andexperiments, Opt. Eng. 55 (2016) 011002, https://doi.org/10.1117/1.OE.55.1.011002.
[9] M. Mitra, S. Gopalakrishnan, Guided wave based structural health monitoring: a review, Smart Mater. Struct. 25 (2016) 053001, https://doi.org/10.1088/0964-1726/25/5/053001.
[10] M. Hasanian, C. Lissenden, Second order harmonic GW mutual interactions in plate: vector analysis, numerical simulation, and experimental results, J. Appl. Phys. 122 (2017) 084901, https://doi.org/10.1063/1.4993924.
[11] W. Li, M. Deng, N. Hu, Y. Xiang, Theoretical analysis and experimental observation of freguency mixingresponse of ultrasonic Lamb waves, J. Appl. Phys. 124 (2018) 044901, https://doi.org/10.1063/1.5028536.
[12] W. Li, Y. Cho, Thermal fatigue damage assessment in an isotropic pipe using nonlinear ultrasonic guided waves, Exp. Mech. 54 (2014) 1309–1318, https://doi.org/10.1007/s11340-014-9882-2.
[13] M. Li, L. Liu, G. Gao, M. Deng, N. Hu, Y. Xiang, W. Zhu, Response features of nonlinear circumferential guided wave on earlydamage in inner layer of a composite circular tube, Chin. PhyS. B 28 (2019) 044301, https://doi.org/10.1088/1674-1056/28/4/044301.
[14] W. Li, Z. Lan, N. Hu, M. Deng, Modeling and simulation of backward combined harmonic generation induced by one-way mixing of longitudinal ultrasonic guided waves in a circular pipe, Ultrasonics 113 (2021) 106356, https://doi.org/10.1016/j.ultras.2021.106356.
[15] C. Yeung, C.-T. Ng, Nonlinear guided wave mixing in pipes for detection of material nonlinearity, J. Sound Vib. 485 (2020) 115541, https://doi.org/10.1016/i.jsv.2020.115541.
[16] J. Cantrell, Acoustic-radiation stress in solids. I. Theory, Phys. Rev. B 30 (1984) 3214, https://doi.org/10.1103/PhysRevB.30.3214.
[17] P. Nagy, J. Qu, L. Jacobs, Finite-size effects on the quasistatic displacement pulse in a solid specimen with quadratic nonlinearity, J. Acoust. Soc. Am. 134 (2013) 1760–1774, https://doi.org/10.1121/1.4817840.
[18] X. Jacob, R. Takatsu, C. Barrière, D. Royer, Experimental study of the acoustic radiation strain in solids, Appl. Phys. Lett. 88 (2006) 134111, https://doi.org/10.1063/1.2191428.
[19] K. Narasimha, E. Kannan, K. Balasubramaniam, Simplified experimental technique to extract the acoustic radiation induced static strain in solids, Appl. Phys. Lett. 91 (2007) 134103, https://doi.org/10.1063/1.2793181.
[20] X. Wan, P. Tse, X. Zhang, G. Xu, Q. Zhang, H. Fan, Q. Mao, M. Dong, C. Wang, H. Ma, Numerical study on static component generation from the primary Lamb waves propagating in a plate with nonlinearity, Smart Mater. Struct. 27 (2018) 045006, https://doi.org/10.1088/1361-665X/aaafeb.
[21] C. Jiang, W. Li, M. Deng, C.-T. Ng, Quasistatic pulse generation of ultrasonic guided waves propagation in composites, J. Sound Vib. 524 (2022) 116764, https://doi.org/10.1016/j.jsv.2022.116764.
[22] C. Jiang, C. Zhang, W. Li, M. Deng, C.-T. Ng, Assessment of damage in composites using static component generation of ultrasonic guided waves, Smart Mater. Struct. 31 (2022) 045025, https://doi.org/10.1088/1361-665X/ac5a77.
[23] W. Li, C. Jiang, J. Xiao, C. Xu, M. Deng, Assessment of thermal damage in polymethyrylate using quasi-static components of ultrasonic waves, J. Nondestr. Eval. 42 (2023) 13, https://doi.org/10.1007/s10921-023-00923-3.
[24] X. Yu, M. Ratassepp, Z. Fan, Damage detection in quasi-isotropic composite bends using ultrasonic feature guided waves, Compos. Sci. Technol. 141 (2017) 120–129, https://doi.org/10.1016/j.compscitech.2017.01.011.
[25] P. Zuo, Z. Fan, SAFE-PML approach for modal study of waveguideswith arbitrary cross sections immersed in inviscid fluid, J. Sound Vib. 406 (2017) 181–196, https://doi.org/10.1016/j.jsv.2017.06.001.
[26] J. Zhao, V. Chillara, B. Ren\, H. CHo, J. Qiu, al e, Second harmonic generation in composites: theoretical and numerical analyses, J. Appl. Phys 119 (2016) 064902, https://doi.org/10.1063/1.4941390.
[27] C. Jiang, W. Li, C.-T. Ng, M. Deng, Quasistatic Component Generation of Group Velocity Mismatched Guided Waves in Tubular Structures for Microdamage Localization, SSRN Electron. J. (2023), https://doi.org/10.2139/ssrn.4398162.
[28] X. Wan, G. Xu, Q. Zhang, P. Tse, H. Tan, A quantitative method for evaluating numerical simulation accuracy of time-transient Lamb wave propagation with its applications to selecting appropriate element size and time step, Ultrasonics 64 (2016) 25–42, https://doi.org/10.1016/j.ultras.2015.07.007.
[29] J.-Y. Kim, L.J. Jacobs, J. Qu, J.W. Littles, Experimental characterization of fatigue damage in a nickel-base superalloy using nonlinear ultrasonic waves, J. Acoust. Soc. Am. 120 (2006) 1266–1273, https://doi.org/10.1121/1.2221557.
[30] J.Y. Kim, J. Qu, L.J. Jacobs, J.W. Littles, M.F. Savage, Acoustic Nonlinearity Parameter Due to Microplasticity, J. Nondestr. Eval. 25 (2006) 28–36, https://doi.org/10.1007/s10921-006-0004-7.
[31] D.S. Forsyth, S.O. Kasap, I. Wacker, S. Yannacopoulos, Thermal fatigue of composites: ultrasonic and SEM evaluations, J. Eng. Mater. Technol. 116 (1) (1994) 113–120, https://doi.org/10.1115/1.2904246.
[32] M.D. Seale, B.T. Smith, W.H. Prosser, Lamb wave assessment of fatigue and thermal damage in composites, J. Acoust. Soc. Am. 103 (1998) 2416–2424, https://doi.org/10.1121/1.422761.
[33] W. Li, Y. Cho, J.D. Achenbach, Detection of thermal fatigue in composites by second harmonic Lamb waves, Smart Mater. Struct. 21 (2012) 085019, https://doi.org/10.1088/0964-1726/21/8/085019.
[34] W. Li, C. Jiang, X. Qing, L. Liu, M. Deng, Assessment of low-velocity impact damage in composites by the measure of secondharmonic guided waves with the phase-reversal approach, Sci. Prog. 103 (2020) 1–14, https://doi.org/10.1177/0036850419881079.